A Proposal for a High-Frequency Earthquake Magnitude (m_{3Hz}) for Seismic Hazard and Rapid Damage Assessment

Stefano Parolai[*1], Daniele Spallarossa[2], Adrien Oth[3], and Matteo Picozzi[4,5]

Abstract

Obtaining a size estimate of an earthquake that well represents its potential impact is of primary importance in seismology and earthquake engineering. The magnitude scales currently used in earthquake catalogs, mainly M_s and M_w, are not designed to represent the variability of shaking due to variations in high-frequency radiation. Conversely, M_L, which best describes the seismic-wave energy released by an earthquake, is unable to provide an accurate representation of events with magnitudes exceeding approximately 6.5. Therefore, building on and extending the concept of high-frequency magnitude (Atkinson and Hanks, 1995), we propose in this article a new high-frequency magnitude scale m_{3Hz}. This magnitude is estimated by also considering correction factors for the crustal model and site effects. We apply the new magnitude scale m_{3Hz} to two data sets (Central Italy and Japan) and validate its ability to capture high-frequency radiation effects through comparison with available source parameters. Finally, a procedure for estimating m_{3Hz} is also proposed for preinstrumental earthquakes. This procedure addresses a limitation of previous magnitude estimation techniques, such as M_e, and is validated for four events for which both macroseismic and instrumental intensity data are available.

Cite this article as Parolai, S., D. Spallarossa, A. Oth, and M. Picozzi (2024). A Proposal for a High-Frequency Earthquake Magnitude (m_{3Hz}) for Seismic Hazard and Rapid Damage Assessment, *Seismol. Res. Lett.* **XX**, 1–10, doi: 10.1785/0220240226.

Introduction

Estimating the size of an earthquake is one of the main goals of seismology and is of fundamental importance, in particular for earthquakes of magnitude > 4, in improving short- and long-term seismic hazard assessment. Since the first definition of magnitude (Richter, 1935), several approaches have been proposed to characterize earthquake strength, based on the analysis of different parts of a seismogram and taking into consideration the technical evolution of seismological equipment (Bormann, 2012). The well-known limitation of the standard surface- and body-wave magnitudes (e.g., M_s by Gutenberg, 1945, and m_b by Gutenberg and Richter, 1956) and those of the local magnitude M_L to correctly estimate the magnitude of strong to major earthquakes (generally referred to as "saturation," e.g., Bormann, 2012) pushed to define the physically based moment magnitude scale M_w (Kanamori, 1977), which, being related to the average static displacement on the rupture and on the area that slipped and estimated at a zero frequency, allows us to overcome this problem. This, together with the possibility of also applying it to historical earthquakes through geological considerations, makes M_w the most suitable characterization of earthquake strength for seismic hazard assessment applications. However, recent works (e.g., Bormann and Di Giacomo, 2011; Picozzi *et al.*, 2019) have shown that M_w cannot capture all characteristics related to earthquake ruptures and in particular may not be an adequate descriptor of radiated energy in the frequency range of interest for most building structures.

To also account for high-frequency radiation in earthquake size estimation, the energy magnitude M_e (Choy and Boatwright, 1995; Newman and Okal, 1998), which considers the integral of the ground-motion velocity, has been proposed for teleseismic recordings. It follows that this estimate, due to the frequency-band narrowness of these recordings, can directly capture high-frequency changes up to a maximum frequency of 1–2 Hz. Trifunac (2008) proposed energy estimation using strong-motion data; however, the limited nature of the observations, which would cover only a portion of the volume affected by seismic-wave propagation, could lead to a bias in the estimated values. Furthermore, the lack of clear relationships between geological information (e.g., average dislocation

1. University of Trieste, Trieste, Italy, https://orcid.org/0000-0002-9084-7488 (SP); 2. University of Genova, Genova, Italy, https://orcid.org/0000-0002-8021-3908 (DS); 3. European Center for Geodynamics and Seismology, Walferdange, Luxembourg, https://orcid.org/0000-0003-4859-6504 (AO); 4. National Institute of Oceanography and Applied Geophysics-OGS, Sgonico, Italy, https://orcid.org/0000-0001-8078-9416 (MP); 5. University of Naples Federico II, Naples, Italy

*Corresponding author: stefano.parolai@units.it

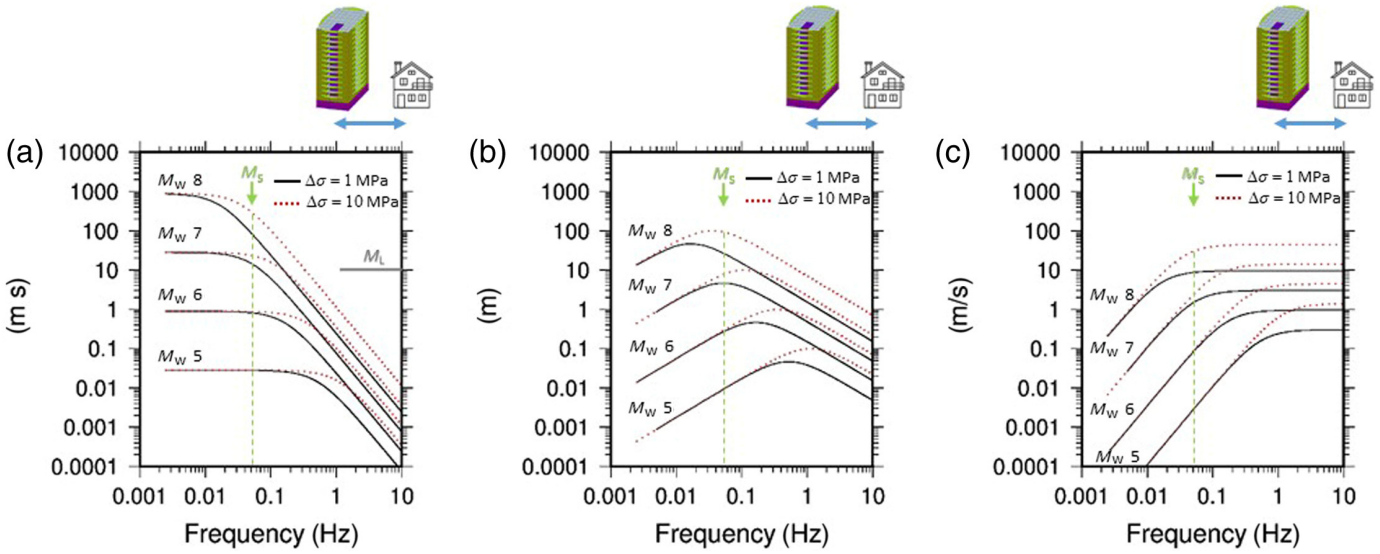

Figure 1. Panels (a–c) Earthquake source spectra in displacement, velocity, and acceleration, respectively. The black lines indicate the source spectra calculated considering a stress drop of 1 MPa. The red lines show the source spectra calculated considering a stress drop of 10 MPa. The frequency band of interest for most of the building is indicated on the top of each panel by a blue line. The green arrow indicates the frequency around which M_s is estimated. The gray line in (a) indicates the frequency band over which M_L is calculated, which is based on the maximum amplitude measured on records from the standardized short-period Wood–Anderson seismometer, which is displacement proportional at frequencies higher than 1.25 Hz (Bormann, 2012). The color version of this figure is available only in the electronic edition.

on the fault) and the radiated energy makes the computation of M_e difficult for historical earthquakes.

Atkinson and Hanks (1995) introduced a high-frequency magnitude **m** that is estimated using a random or logarithmically averaged horizontal component of ground motion from frequencies above the highest corner frequency of the earthquake source spectrum at a hypocentral or closest fault distance of 10 km. The scale was arranged to provide **m** consistent to M_w for events of "average" stress drop in both eastern North America and California. Atkinson and Hanks (1995) proposed a relationship between **m** and the modified Mercalli intensities, providing a link between engineering ground-motion parameters and intensity data, which makes **m** useful also for large preinstrumental earthquakes.

However, being calibrated in the high-frequency level of the Fourier spectrum of acceleration, in its original formulation, the estimation of **m** is highly sensitive to site effects that can lead to large single-station estimation values. In fact, in terms of their magnitude definition, an average spectral amplification of 3 in the frequency band under consideration results in an increase in magnitude of 1.

In this study, considering the definition of **m** by Atkinson and Hanks (1995), it is proposed to estimate the size of an earthquake (at local or regional distances) using the spectral amplitude of acceleration at 3 Hz($\mathbf{m}_{3Hz}$), introducing correction factors for propagation distance, site effects, and for the differences between the average velocity of the adopted crustal model used to generate the theoretical source spectra and that of the reference site used for estimating site response. $\mathbf{m}_{3Hz}$ is proposed with the goal of complementing M_w for seismic hazard and rapid damage assessment.

Unlike Atkinson and Hanks (1995), an absolute reference for anchoring $\mathbf{m}_{3Hz}$ to M_w is used. We present $\mathbf{m}_{3Hz}$ estimates for two data sets (Central Italy and Japan), for which independent estimates of M_w are available, and the results will be discussed in terms of the importance of high-frequency radiation with respect to earthquake size.

Finally, we also show the implementation of $\mathbf{m}_{3Hz}$ for four significant earthquakes that occurred in Central Italy for which macroseismic (Locati *et al.*, 2022) and instrumental intensity data information support the application of $\mathbf{m}_{3Hz}$ for revisiting the size estimates of large earthquakes in historical catalogs.

Definition $\mathbf{m_{3Hz}}$

Considering the well-known ω^{-2} single corner-frequency source spectral model (e.g., Brune, 1970, 1971), the spectral amplitude of two earthquakes with a difference of 1 unit in M_w differs at the frequency 0 Hz by almost a factor of 30 (31.6), which gives rise to the factor of 2/3 applied to the logarithm of the seismic moment M_0 in the classical relationship of Hanks and Kanamori (1979). However, considering the case for which the two earthquakes share the same value of the stress drop, the high-frequency spectral amplitude will tend to a ratio of nearly 3.2 (3.17) (Fig. 1). Figure 1 shows that the 3 Hz Fourier spectral amplitudes are still in the flat part of the acceleration spectrum (for the range of the considered stress drops) for earthquakes larger than M_w 5 (and probably also for M_w 4)

and thus provide a linear scaling (logarithmic scale) between different earthquakes. The 3 Hz frequency is also low enough to be far from the typical f_{max} values ranging between 10 and 20 Hz (Hanks, 1982) and well within the frequency band of interest for shaking capable of damaging residential buildings (ranging for most of them between 1 and 10 Hz). It follows that the spectral amplitude variation at this frequency, which can also be picked out easily in spectra calculated quickly after a seismic event, can well represent seismic radiation in the range of frequencies that affect the structural behavior of buildings and is therefore suitable for seismic hazard assessment.

Finally, and importantly, Figure 1 shows that for the same seismic moment, a change of a factor of 10 in the stress drop (here the values for 1 and 10 MPa are represented consistent with the range for which M_w was proposed in Hanks and Kanamori, 1979) leads to spectral amplitudes in the high-frequency range that are compatible with (or slightly larger than) those expected for an $M_w + 1$ earthquake.

Following a classical approach in defining a magnitude scale, and based on what has been written so far in this section, $\mathbf{m}_{3Hz}$ is defined as

$$\mathbf{m}_{3Hz} = 2\log\left(\frac{A}{A_o}\right) + 2\log\left(\frac{D}{D_0}\right) + 5 + \Delta_{anel} - \Delta_{site} - \Delta_{site_{ref}}, \quad (1)$$

in which A is the larger of the two spectral amplitudes measured at 3 Hz of the two horizontal components of the acceleration (in meters per second), A_0 is the reference spectral amplitude at 3 Hz of the source function of the single corner frequency model at 10 km, obtained considering an M_w 5 event and assuming a stress drop equal to 1 MPa. In our case a ω^{-2} model was assumed, and the shear-wave velocity was set to 3500 m/s, leading to a value of 0.029525 m/s. In the second term of equation (1), D is the hypocentral distance (km) and D_0 is the reference distance equal to 10 km. Δ_{anel} is an empirically estimated correction factor for each earthquake to account for a possible path-dependent correction of anelastic attenuation from the 10 km magnitude estimates. Δ_{site} is the site amplification factor, estimated as two times the logarithm of the site amplification at 3 Hz, estimated from site response with respect to a reference site. $\Delta_{site_{ref}}$ is the reference site amplification factor, accounting for the difference in impedance between the velocity in the shallow crustal layer at the reference station (V_r) and the adopted velocity model (V_m), and it is calculated similarly to the square root impedance amplification (Boore, 2013) as

$$\Delta_{site_{ref}} = 2\log\left(\frac{V_m}{V_r}\right). \quad (2)$$

It is observed that the decision to utilize the maximum value of the components, although based on spectra, aligns with the original definition of magnitude. However, it might still be preferable to calculate the magnitude independently for the two components and then average the two results. In addition, the shaking maxima on the two components may not occur at the same time and may not represent the same phase (Bormann, 2012) in both the time and frequency domains. Considering the potential applications in seismic hazard estimation, it is proposed that the maximum value on one of the two horizontal components be utilized as a preliminary and conservative approach.

Finally, it is important to note that based on the aforementioned observations and the first term in equation (1), namely that a change in amplitude of spectral acceleration by a factor of 3 corresponds to an increase of one unit in magnitude, it is important to remove the site effects' influence. Indeed, even minor spectral amplifications due to local geology can result in significant changes in magnitude.

Procedure for Estimating $\mathbf{m_{3Hz}}$

The procedure adopted in this study, which can also be easily implemented for real-time data analysis, consists of the following steps:

1. calculating the Fourier transform of an *S*-wave window of the horizontal component of ground motion, which starts before the arrival of the *S* wave and includes the largest amplitude of the ground motion at each station;
2. smoothing of spectra using a Konno and Ohmachi logarithmic window (Konno and Ohmachi, 1998) with the coefficient b, which determines the bandwidth (2.6–3.5 Hz, around 3Hz), fixed at 40. This approach ensures the smoothing of numerical instabilities while preserving the major features of the spectra;
3. selection of spectral amplitude at the frequency closest to 3 Hz (A). The maximum of the two horizontal component is selected;
4. first calculation of $\mathbf{m}_{3Hz}$ magnitude considering the hypocentral distance D, the precalculated site amplification at 3 Hz (e.g., from generalized inversion technique [GIT] analysis, Anderson, 1986) Δ_{site}, and the $\Delta_{site_{ref}}$. The Δ_{site} factor being obtained from GIT considers 1D, 2D, and 3D effects;
5. the linear trend affecting the station estimates of the $\mathbf{m}_{3Hz}$ magnitude with respect to the hypocentral distance is removed to eliminate any potential bias with respect to the $\mathbf{m}_{3Hz}$ at a distance of 10 km(Δ_{anel}); and
6. estimation of the $\mathbf{m}_{3Hz}$ event as the average value of those of the stations and calculation of the standard deviation. In this study, the simple mean is employed for simplicity and to assess the dispersion of the values, even after path and site corrections have been carried out. Other approaches, such as the trimmed mean, can be considered for calculating the average value and reducing the dispersion of the obtained estimates.

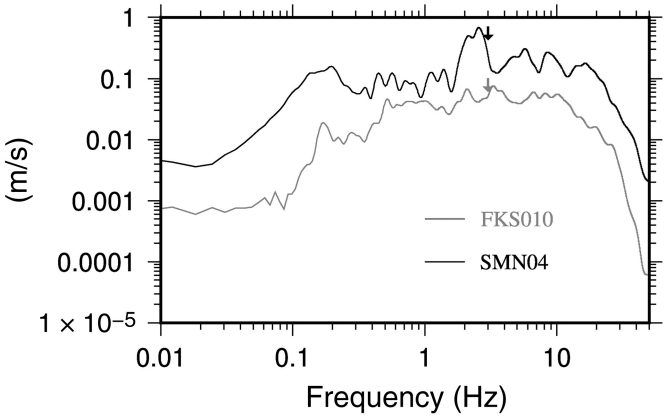

Figure 2. The black line represents the Fourier spectrum of the acceleration recording of the ID 0010061330 (Table A1 in the Appendix) earthquake at the SMN04 station, situated 42 km from the epicenter. Following the application of a site term correction, the station $\mathbf{m_{3Hz}}$ was found to be 7.2, whereas the M_w was estimated to be equal to 6.6. The black arrow indicates the frequency of 3 Hz. The gray line represents the Fourier spectrum of the acceleration recording of the ID 1106182031 (Table A1 in the Appendix) earthquake at station FSK010, located at 88 km from the epicenter. The station $\mathbf{m_{3Hz}}$ is 6.0, after site term correction, whereas the estimated M_w was 6.1. The gray arrow indicates the frequency of 3 Hz.

Application to Two Test Cases

Japan data set

The $\mathbf{m_{3Hz}}$ is calculated for a data set of 16 earthquakes recorded by the K-NET and KiK-net networks (Japan; Okada *et al.*, 2004) with M_w ranging between 5.7 and 6.9. A total of 2858 Fourier spectra of horizontal component of ground motion are analyzed. The accelerograms of these earthquakes were previously used in a nonparametric spectral inversion scheme by Oth *et al.* (2011), which allowed the derivation of attenuation characteristics, source spectra, and site response. This data set was also used for testing decentralized onsite earthquake early warning systems in Parolai *et al.* (2017). The stress-drop estimation of these events was later revised by Oth (2013) and its relationship with ground-motion variability studied by Oth *et al.* (2017), and ranges between 2.2 and 14.8 MPa. Figure 2 depicts, as an example, the outcomes of acceleration spectra calculations for two events (IDs 0010061330 and 1106182031, Table A1 in the Appendix) recorded at epicenter distances of 42 and 88 km, respectively. The shape of the spectrum, with clear peaks at frequencies above 1 Hz, is indicative of the significance of the site correction, which represents approximately a unit of magnitude in both cases, in determining $\mathbf{m_{3Hz}}$.

Figure 3 illustrates that when the estimated stress drop exceeds the reference value of 1 MPa, there is a discernible tendency for $\mathbf{m_{3Hz}}$ to be larger than M_w. The depicted event-averaged values were obtained following the point (6) of the proposed procedure.

In the case of the largest stress-drop events, the difference can even reach a value of 1.5. Moreover, although the limited data set does not permit definitive conclusions, Figure 4 illustrates a positive correlation between the differences between $\mathbf{m_{3Hz}}$ and M_w and the logarithm of the stress drop. The figure shows only a weak correlation, which does not allow for definitive conclusions given the number of data analyzed here. Remarkably, despite the adopted corrections, the precision in the estimates measured through the standard deviation is of the order of 0.45.

Central Italy data set

For this section, we analyzed 3300 spectra belonging to 34 earthquakes with $4.5 \le M_w \le 6.5$ ($4.4 \le M_L \le 6.1$) that occurred in Central Italy between 2009 and 2023 and were recorded by 181 stations (Table A1 in the Appendix). The M_L computation is performed by measuring peak amplitudes of synthetic Wood–Anderson seismograms (Di Bona, 2016). The Δ_{site} terms were estimated using the GIT technique (Anderson, 1986) applied to a larger data set made of 2377 events and 631 stations. A nonparametric approach (Castro *et al.*, 1990) was used. Considering the results of Lanzano *et al.* (2022), based on a careful analysis of geological and geophysical data, the station FIAM has been considered as the reference station (V_{S30} approximately of 1000 m/s).

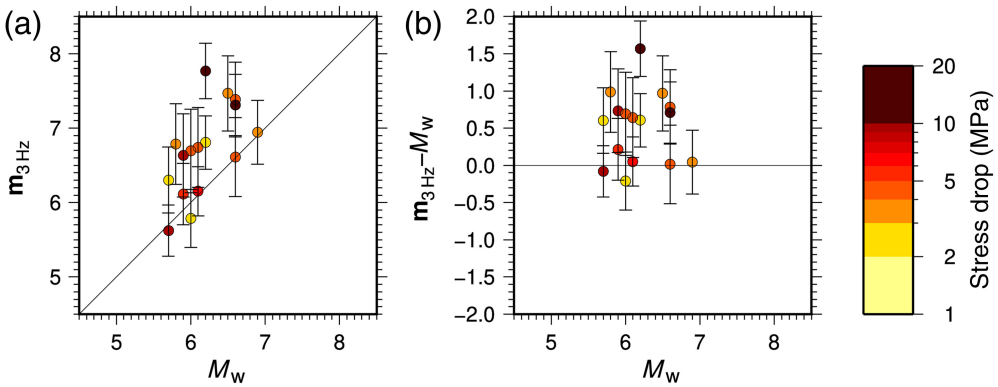

Figure 3. (a) Estimated $\mathbf{m_{3Hz}}$ versus M_w for the K-NET and KiK-net data (Japan). Symbol colors indicate the stress drop in MPa. (b) Differences between $\mathbf{m_{3Hz}}$ and M_w versus M_w. Black bars indicate the standard deviation of the estimate. The color version of this figure is available only in the electronic edition.

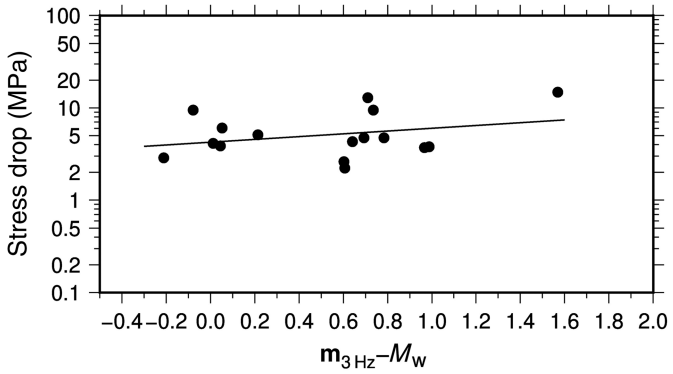

Figure 4. Stress drop versus ($\mathbf{m}_{3Hz} - M_w$) for the Japanese data set. The optimal fit line in the least-squares sense is represented by the equation $\log_{10}(\Delta\sigma) = a + b\Delta m$, in which $\Delta\sigma$ is the stress drop and Δm is the difference between $\mathbf{m}_{3Hz}$ and M_w. This leads to a = 0.63 ± 0.09 and b = 0.15 ± 0.13.

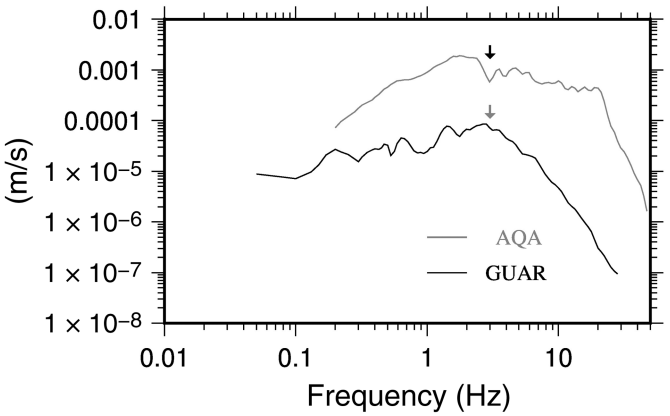

Figure 5. The gray line represents the Fourier spectrum of the acceleration recording of the ID 090409005259, M_w 5.2 (Table A1 in the Appendix) earthquake at the AQA station, located 15 km from the hypocenter. The black line represents the Fourier spectrum of the acceleration recording of the earthquake at station GUAR, located at 88 km from the epicenter.

Figure 5 illustrates the results of acceleration spectra calculations for an event (ID 090409005259, Table A1 in the Appendix) recorded at epicentral distances of 15 km (AQA station) and 88 km (GUAR station), respectively. The spectra related to rock sites confirm the choice of the 3 Hz frequency as an optimal compromise.

Figure 6 shows that for M_w smaller than 5, the event averaged $\mathbf{m}_{3Hz}$ estimates are consistent with those of M_w, whereas for larger magnitudes, $\mathbf{m}_{3Hz}$ estimates tend to increase. This observation is consistent with the results of Calderoni and Abercrombie (2023), who estimated the stress drop and the rupture complexities for some of the events considered here. Remarkably, their stress-drop estimates are scattered around 1 MPa for M_w 4.5 and increase up to nearly 7 MPa for the largest events. Figure 6 illustrates that M_L tends to provide higher values than M_w for magnitudes less than 5, and it appears to saturate for larger events. However, further in-depth analysis can be conducted on expanded data sets in the future. Finally, it is worth noting that for this data set, despite the adopted corrections, the precision measured trough the standard deviation is of the order of 0.47.

Calculation of $\mathbf{m}_{3Hz}$ from Macroseismic Intensity Data

Assessing the possible application of $\mathbf{m}_{3Hz}$ to macroseismic intensity data is of fundamental importance for its application in seismic hazard assessment procedures. In this regard, the macroseismic fields of four of the events that occurred in Central Italy, and for which $\mathbf{m}_{3Hz}$ was estimated using available strong-motion data (Fig. 3), were considered.

First, macroseismic intensity values were converted to peak ground acceleration (PGA) using the inverse relationship of equation (5) of Oliveti *et al.* (2022). Second, a relationship between PGA and spectral amplitude A at 3 Hz was calculated using the Japanese data set of 2858 records (Fig. 7a), thus avoiding any possible bias due to the usage of data coming from the same region as the tested one.

The relationship is in the form:

$$\log A = a \log(\mathrm{PGA}) + b, \tag{3}$$

in which a = 0.911 ± 0.01 and b = −0.896 ± 0.006.

Finally, equation (3) is applied for each site without considering the Δ_{anel}, Δ_{site}, and $\Delta_{site_{ref}}$ terms both for simplicity and to simulate a situation as close as possible to that of historical data.

The results (Fig. 7b) show a good agreement between the $\mathbf{m}_{3Hz}$ estimated from the strong-motion data and those derived from the macroseismic intensities. Notably, the same trend of variation in magnitude is captured by both approaches.

Discussion and Conclusions

In this article, a new $\mathbf{m}_{3Hz}$ magnitude scale for local and regional earthquake data sets is proposed. The scale provides a linear scaling (logarithmic scale) for events with a magnitude exceeding approximately 4. Being determined considering the high-frequency radiation, it may be particularly effective for seismic hazard estimation. It is worth noting that using an anelastic correction factor that is estimated for each earthquake independently makes the implementation of the $\mathbf{m}_{3Hz}$ particularly suitable for quasi-real-time applications. The results obtained for two data sets (Central Italy and Japan) demonstrated the efficacy of the $\mathbf{m}_{3Hz}$ value in reflecting high-frequency radiation through a comparison with available estimates of the stress drop for the events under consideration. Based on the experience of future applications, the

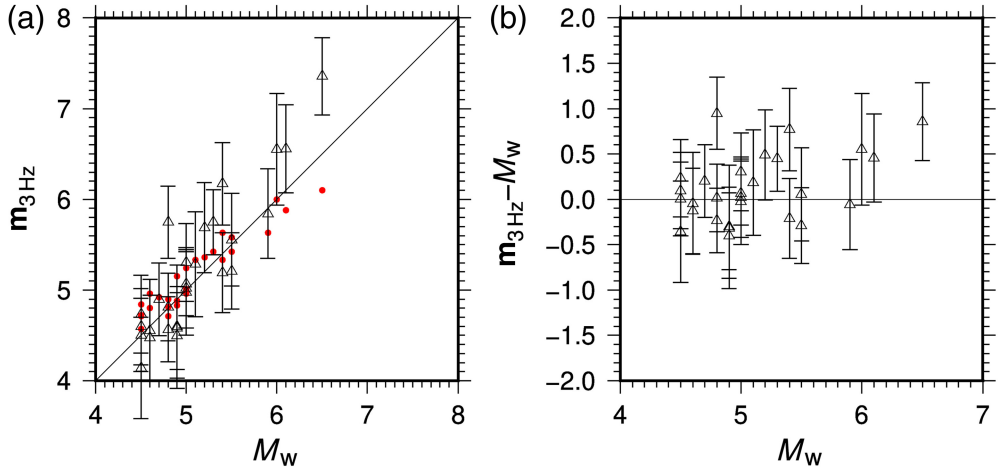

Figure 6. (a) Estimated $\mathbf{m}_{3Hz}$ (triangles) versus M_W for the Central Italy data set. Red circles indicate M_L versus M_W. (b) Differences between $\mathbf{m}_3$ and M_W versus M_W. Black bars indicate the standard deviation of the estimate. The color version of this figure is available only in the electronic edition.

proposed procedure could be modified in some technical details to reduce the variability of the estimate $\mathbf{m}_{3Hz}$ for an event when averaged over the values calculated for individual stations. For example, a replacement of simple averaging of station values with a trimmed average (eliminating particularly outlier values) could allow a reduction in the final uncertainty. This could also limit the impact of strong variability in the single-station magnitude estimates arising from local rupture effects (e.g., slip distribution) in the case of strong events. Furthermore, in this study we have shown that in the range of magnitudes considered (up to about M_w 6.9) the choice of using the hypocentral distance can be reasonable. However, for major or great events, or for deep events, this choice of metric could be revised by considering alternative distance estimates that can better account for the finiteness of the rupture and thus reduce possible uncertainties in the $\mathbf{m}_{3Hz}$ station estimates. Although the initial considerations brought to support the proposed magnitudes start from a single-corner frequency ω^{-2} model (as in Bormann and Di Giacomo, 2011), tests we conducted showed that even for rupture models on extended faults (Haskell, 1964), the considerations remain essentially valid in the magnitude range considered.

The utilization of $\mathbf{m}_{3Hz}$ necessitates a comprehensive understanding of the site response of the stations relative to a reference site to obtain robust magnitude estimates.

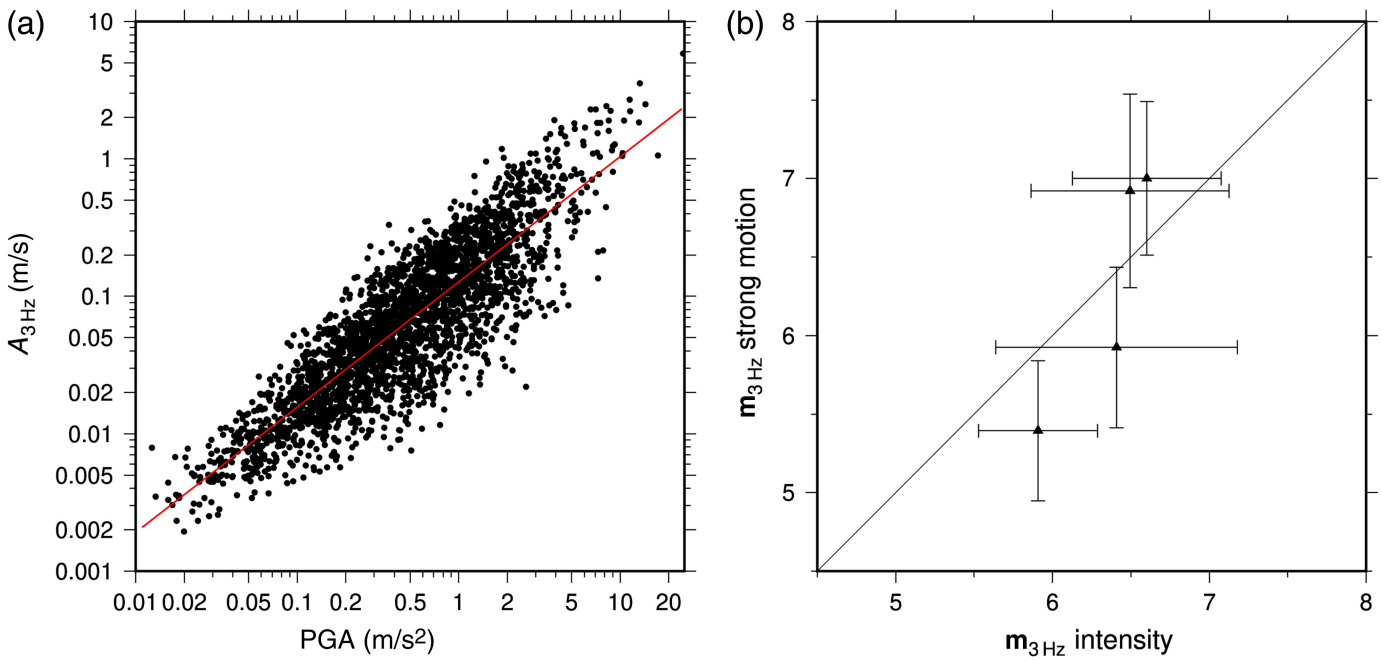

Figure 7. (a) Spectral amplitudes at 3 Hz versus peak ground acceleration (PGA) obtained from the 2858 horizontal-component recordings of the Japanese data set (black dots). The red line indicates the regression of equation (3). (b) $\mathbf{m}_{3Hz}$ obtained by macroseismic intensity data versus $\mathbf{m}_{3\,Hz}$ estimated by strong-motion data and corresponding error bars. The color version of this figure is available only in the electronic edition.

This is a significant advantage over the use of proxies such as V_{S30} for describing the site response, as it considers the physical estimate of it. However, it may appear to be a limitation for networks that lack such knowledge. It is important that, given the current availability and sharing of data, the estimation of site response, including through GIT, is no longer limited to the individual network, regional, or national level. In fact, recent work in Europe has made site-response functions available at a pan-European scale (Bindi *et al.*, 2023; Yen *et al.*, 2024).

Consequently, the implementation of $\mathbf{m_{3Hz}}$ at European scale would be a viable option, enhancing the value of site-response studies. In addition, although 3 Hz corrections are not yet available for all networks, they may become so quickly because GIT application is becoming a routine procedure. However, we would like to mention that a proper implementation of M_L and in such cases M_w (see Scognamiglio *et al.*, 2016) still requires the estimation of station corrections or ad hoc near-surface velocity models. The $\mathbf{m_{3Hz}}$ magnitude could also be computed without proper knowledge of the 3 Hz site amplification (if not available), using either only rock stations or all stations, then limiting any bias by eliminating those that give very different values (outliers) due to site amplification.

With respect to other magnitude scales that well reflect high-frequency radiation (e.g., M_e), the added value of $\mathbf{m_{3Hz}}$ is that it can also be estimated for preinstrumental earthquakes.

In this regard, a procedure for estimating $\mathbf{m_{3Hz}}$ has been proposed that has been validated using macroseismic data from earthquakes, for which strong-motion recordings are also available. The obtained values of $\mathbf{m_{3Hz}}$ from macroseismic intensity data are in good agreement with those estimated from strong-motion data, exhibiting similar precision of estimation (0.4–0.5), and the same trend in defining the relative size of events.

Future studies will focus on developing earthquake catalogs (preinstrumental and instrumental) using $\mathbf{m_{3Hz}}$ and, therefore, developing new ground-motion relationships, in particular taking advantage of the numerous GIT studies carried out both at regional and national level. It is anticipated that $\mathbf{m_{3Hz}}$ may offer a more accurate representation of high-frequency ground-motion variability than the currently employed magnitude scales. This could potentially lead to a reduction in the scatter of ground-motion intensity measurement values in ground-motion models, a finding that warrants further investigation. In fact, the expected reduction in variability, currently considered random in ground-motion prediction equations, could facilitate the development of more accurate seismic hazard models.

Importantly, real-time or near-real-time computation of $\mathbf{m_{3Hz}}$, will be implemented within Ramones (Spallarossa *et al.*, 2021) so as to enable more effective assessment of the impact of earthquake events at the Italian level and, in the future, at the European level.

Data and Resources

The data set used in this study was collected from multiple sources to ensure comprehensive coverage and accuracy. For the Japanese data set, seismic records were acquired from the National Research Institute for Earth Science and Disaster Resilience (NIED) in Japan. Data can be obtained from the K-NET and KiK-net websites at http://www.kyoshin.bosai.go.jp/ (last accessed August 2017). For the Italian data set, records and parametric information were retrieved from the Observatories and Research Facilities for European Seismology (ORFEUS) European Integrated Data Archive (EIDA; https://www.orfeus-eu.org/data/eida/, last accessed August 2023), the Incorporated Research Institutions for Seismology (IRIS; https://www.iris.edu/hq/, last accessed August 2023), and the Italian Civil Protection Department (http://ran.protezionecivile.it/EN/index.php, last accessed August 2023). The National Institute for Geophysics and Volcanology (INGV) bulletin is used to guide the data download (webservices.rm.ingv.it/fdsnws/event/1/, last accessed September 2020) and to extract the earthquake parameters. The International Federation of Digital Seismograph Networks (FDSN) specifications are available at http://www.fdsn.org/ (last accessed August 2023) and the Standard for the Exchange of Earthquake Data manual is available at http://www.fdsn.org/pdf/SEEDManual_V2.4.pdf (last accessed February 2021). The seismic recordings utilized in this study primarily originate from the following seismic monitoring networks: INGV (doi: 10.13127/SD/XOFXnH7QfY), Presidency of Council Of Ministers-Civil Protection Department (doi: 10.914/SN/IT), MedNet Project Partner Institutions, doi: 10.13127/SD/fBBBtDtd6q), University Of Bari "Aldo Moro" (doi: 10.7914/SN/OT), Armatrice Sequence International (doi: 10.7914/SN/YR_2016), Rete sismica del gruppo EMERSITO (doi: 10.13127/SD/7TXeGdo5X8), Seismic network RESIF-SISMOB (doi: 10.15778/RESIF.XJ2009) and 3A (Rete del Centro di Microzonazione Sismica (CentroMZ; doi: 10.13127/SD/ku7Xm12Yy9). The intensity data for the four seismic events utilized in this study were obtained from the Database Macrosismico Italiano (DBMI15), version 4.0 (https://emidius.mi.ingv.it/CPTI15-DBMI15/, last accessed March 2023).

Declaration of Competing Interests

The authors acknowledge that there are no conflicts of interest recorded.

Acknowledgments

This study was partially funded by the Joint Research Unit (JRU) of European Plate Observing System infrastructure (EPOS) Italia (https://www.epos-italia.it/, last accessed September 2024). The figures were drawn using the Generic Mapping Tools (GMT, Wessel *et al.*, 2019) software.

References

Anderson, J. G. (1986). Implication of attenuation for studies of the earthquake source, in *Earthquake Source Mechanics*, S. Das and J. Boatwright (Editors), American Geophysical Union, Washington, D.C., 311–318.

Atkinson, G. M., and T. Hanks (1995). A high-frequency magnitude scale, *Bull. Seismol. Soc. Am.* **85,** no. 3 825–833.

Bindi, D., R. Zaccarelli, H. N. T. Razafindrakoto, M. H. Yen, and F. Cotton (2023). Empirical shaking scenarios for Europe: A feasibility study, *Geophys. J. Int.* **232,** 990–1005.

Boore, D. M. (2013). The uses and limitations of the square-root impedance method for computing site amplification, *Bull. Seismol. Soc. Am.* **103,** 2356–2368.

Bormann, P. (Editor) (2012). *New Manual of Seismological Observatory Practice (NMSOP-2)*, Deutsches GeoForschungszentrum GFZ, Potsdam, Germany, doi: 10.2312/GFZ.NMSOP-2.

Bormann, P., and D. Di Giacomo (2011). The moment magnitude Mw and the energy magnitude Me: Common roots and differences, *J. Seismol.* **15,** 411–427, doi: 10.1007/s10950-010-9219-2.

Brune, J. N. (1970). Tectonic stress and the spectra of the seismic shear waves from earthquakes, *Geophys. Res. Lett.* **75,** 4997–5009.

Brune, J. N. (1971). Correction, *J. Geophys. Res.* **76,** no. 20, 5002.

Calderoni, G., and R. E. Abercrombie (2023). Investigating spectral estimates of stress drop for small to moderate earthquakes with heterogeneous slip distribution: Examples from the 2016-2017 Amatrice earthquake sequence, *J. Geophys. Res.* **128,** e2022JB025022, doi: 10.1029/2022JB025022.

Castro, R. R., J. G. Anderson, and S. K. Singh (1990). Site response, attenuation, and source spectra of S-waves along the Guerrero, Mexico, subduction zone, *Bull. Seismol. Soc. Am.* **80,** 1481–1503.

Choy, G. L., and J. L. Boatwright (1995). Global patterns of radiated seismic energy and apparent stress, *J. Geophys. Res.* **100,** no. B9, 18,205–18,228.

Di Bona, M. (2016). A local magnitude scale for crustal earthquakes in Italy, *Bull. Seismol. Soc. Am.* **106,** 242–258, doi: 10.1785/0120150155.

Gutenberg, B. (1945). Amplitudes of surface waves and magnitudes of shallow earthquakes, *Bull. Seismol. Soc. Am.* **35,** 3–12.

Gutenberg, B., and C. F. Richter (1956). Magnitude and energy of earthquakes, *Ann. Geofis.* **9,** 1–15.

Hanks, T. C. (1982). f max, *Bull. Seismol. Soc. Am.* **72,** no. 6A, 1867–1879, doi: 10.1785/BSSA07206A1867.

Hanks, T. C., and H. Kanamori (1979). A moment magnitude scale, *J. Geophys. Res.* **84,** no. B5, 2348–2350.

Haskell, N.-A. (1964). Total energy and energy spectral density of elastic wave radiation from propagating faults, *Bull. Seismol. Soc. Am.* **54,** no. 6A, 1811–1841, doi: 10.1785/BSSA05406A1811.

Kanamori, H. (1977). The energy release in great earthquakes, *J. Geophys. Res.* **82,** 2981–2987.

Konno, K., and T. Ohmachi (1998). Ground-motion characteristics estimated from spectral ratio between horizontal and vertical components of microtremors, *Bull. Seismol. Soc. Am.* **88,** 228–241.

Lanzano, G., C. Felicetta, F. Pacor, D. Spallarossa, and P. Traversa (2022). Generic-to reference rock scaling factors for seismic ground motion in Italy, *Bull. Seismol. Soc. Am.* **112,** 1583–1606, doi: 10.1785/0120210063.

Locati, M., R. Camassi, A. Rovida, E. Ercolani, F. Bernardini, V. Castelli, C. H. Caracciolo, A. Tertulliani, A. Rossi, R. Azzaro, *et al.* (2022). Database Macrosismico Italiano (DBMI15), versione 4.0, *Istituto Nazionale di Geofisica e Vulcanologia (INGV)*, doi: 10.13127/dbmi/dbmi15.4.

Newman, A. V., and E. A. Okal (1998). Teleseismic estimates of radiated seismic energy: The E/M_0 discriminant for tsunami earthquakes, *J. Geophys. Res.* **103,** no. B11, 26,885–26,898, doi: 10.1029/98JB02236.

Okada, Y., K. Kasahara, S. Hori, K. Obara, S. Sekiguchi, H. Fujiwara, and A. Yamamoto (2004). Recent progress of seismic observation networks in Japan-Hi-net, F-net, K-NET and KiK-net, *Earth Planets Space* **56,** 15–28.

Oliveti, I., L. Faenza, and A. Michelini (2022). New reversible relationships between ground motion parameters and macroseismic intensity for Italy and their application in ShakeMap, *Geophys. J. Int.* **231,** no. 2, 1117–1137, doi: 10.1093/gji/ggac245.

Oth, A. (2013). On the characteristics of earthquake stress release variations in Japan, *Earth Planet. Sci. Lett.* **377,** 132–141, doi: 10.1016/j.epsl.2013.06.037.

Oth, A., D. Bindi, S. Parolai, and D. Di Giacomo (2011). Spectral analysis of K-NET and KiK-net data in Japan, part II: On attenuation characteristics, source spectra, and site response of borehole and surface stations, *Bull. Seismol. Soc. Am.* **101,** 667–687, doi: 10.1785/0120100135.

Oth, A., H. Miyake, and D. Bindi (2017). On the relation of earthquake stress drop and ground motion variability, *J. Geophys. Res.* **122,** 5474–5492, doi: 10.1002/2017JB014026.

Parolai, S., A. Oth, and T. Boxberger (2017). Performance of the GFZ Decentralized On-Site Earthquake Early Warning Software (GFZ-Sentry): Application to K-NET and KiK-Net Recordings, Japan, *Seismol. Res. Lett.* **88,** no. 6, 1480–1490, doi: 10.1785/0220170048.

Picozzi, M., D. Bindi, D. Spallarossa, A. Oth, D. Di Giacomo, and A. Zollo (2019). Moment and energy magnitudes: Diversity of views on earthquake shaking potential and earthquake statistics, *Geophys. J. Int.* **216,** no. 2, 1245–1259.

Richter, C. (1935). An instrumental earthquake magnitude scale, *Bull. Seismol. Soc. Am.* **25,** 1–32.

Scognamiglio, L., F. Magnoni, E. Tinti, and E. Casarotti (2016). Uncertainty estimations for moment tensor inversions: the issue of the 2012 May 20 Emilia earthquake, *Geophys. J. Int.* **206,** no. 2, 792–806.

Spallarossa, D., M. Picozzi, D. Scafidi, P. Morasca, C. Turino, and D. Bindi (2021). RAMONES, the Rapid Assessment of MOmeNt and Energy Service in Central Italy: Concepts, capabilities and future perspectives, *Seismol. Res. Lett.* doi: 10.1785/0220200348.

Trifunac, M. D. (2008). Energy of strong motion at earthquake source, *Soil Dynam. Earthq. Eng.* **28,** no. 1, 1–6, doi: 10.1016/j.soildyn.2007.06.009.

Wessel, P., J. F. Luis, L. Uieda, R. Scharroo, F. Wobbe, W. H. F. Smith, and D. Tian (2019). The Generic Mapping Tools version 6, *Geochem. Geophys. Geosys.* **20,** 5556–5564, doi: 10.1029/2019GC008515.

Yen, M. H., D. Bindi, A. Oth, B. Edwards, R. Zaccarelli, and F. Cotton (2024). Source parameters and scaling relationships of stress drop for shallow crustal seismic events in Western Europe, *J. Seismol.* **28,** 63–79, doi: 10.1007/s10950-023-10188-y.

Appendix

Table A1 provides information on the data set of events (Central Italy and Japan) used in this study. In particular, the IDs, location parameters and estimated magnitudes of the events are given.

TABLE A1
List of the Used Events

Japanese Data Set

Name of Event		ID	Date and Time (yyyy/mm/dd hh:mm:ss.ss)	Latitude (°)	Longitude (°)	Depth (km)	M_{JMA}	M_w	M_L
2005	Fukuoka	0503201053	2005/03/20 10:53:55.29	33.747379	130.173354	11.1	7.0	6.6	
1997	Kagoshima 1	9703261731	1997/03/26 17:32:2.85	31.976218	130.389674	8.2	6.5	6.1	
1997	Kagoshima 2	9705131438	1997/05/13 14:38:42.79	31.938344	130.327643	8.6	6.3	6.0	
2000	Tottori	0010061330	2000/10/06 13:30:32.74	35.292102	133.345385	11.7	7.3	6.6	
		0006070616	2000/06/07 06:16:58.01	36.837000	135.550500	22.0	6.1	5.8	
2003	Miyagi-Oki	0307260713	2003/07/26 07:13:46.53	38.396009	141.180943	12.2	6.4	6.1	
2004	Mid-Niigata	0410231756	2004/10/23 17:56:15.16	37.291018	138.858914	12.7	6.8	6.5	
2004	Mid-Niigata 2	0410231803	2004/10/23 18:03:28.12	37.343391	138.972135	10.1	6.3	6.0	
2004	Mid-Niigata 3	0410231812	2004/10/23 18:12:12.35	37.235795	138.811963	13.7	6.0	5.7	
2004	Mid-Niigata 4	0410231834	2004/10/23 18:34:20.69	37.303300	138.933200	14.1	6.5	6.3	
2004	Mid-Niigata 5	0410271040	2004/10/27 10:41:05.23	37.278906	139.033282	11.0	6.1	5.8	
2007	Noto	0703250942	2007/03/25 09:42:12.79	37.253062	136.680876	19.7	6.9	6.7	
2007	Chuetsu-Oki	0707161013	2007/07/16 10:13:38.09	37.498697	138.664701	20.8	6.8	6.6	
2008	Iwate	0806140843	2008/06/14 08:44:00.31	39.035038	140.890262	6.8	7.2	6.9	
2011	Nakano-Niigata	1103120359	2011/03/12 03:59:30.47	36.981954	138.579594	4.4	6.7	6.2	
		9809031658	1998/09/03 16:58:32.44	39.795700	140.909700	9.6	6.1	5.9	
2009	Shizuoka	0908110507	2009/08/11 05:07:22.43	34.772174	138.500200	25.4	6.5	6.2	
		1103152231	2011/03/15 22:32:01.01	35.303075	138.708767	2.8	6.4	5.9	
		1103161252	2011/03/16 12:52:17.77	35.855765	140.903174	21.8	6.1	5.8	
		1103191856	2011/03/19 18:57:02.70	36.782200	140.601180	7.1	6.1	5.8	
		1103230712	2011/03/23 07:12:43.23	37.078853	140.830310	10.8	6.0	5.7	
		1104121407	2011/04/12 14:07:57.26	37.055518	140.624315	14.3	6.4	5.9	
		1106182031	2011/06/18 20:31:19.61	37.617700	141.821300	27.6	6.0	5.7	
		1108191436	2011/08/19 14:36:45.67	37.632348	141.866213	20.6	6.5	6.3	

Central Italy Data Set

2009	Aquila Sequence	090406013240	2009/04/06 01:32:40,4	42.3625	13.3728	9.9		6.1	5.9
2009	Aquila Sequence	090406013629	2009/04/06 01:36:29,19	42.3603	13.3408	6.6		0.0	4.5
2009	Aquila Sequence	090406023704	2009/04/06 02:37:4,25	42.3737	13.3402	10.0		4.9	4.9
2009	Aquila Sequence	090406231536	2009/04/06 23:15:36,76	42.4772	13.3913	11.1		5.0	5.0
2009	Aquila Sequence	090407092628	2009/04/07 09:26:28,61	42.3383	13.4000	10.0		4.9	4.8
2009	Aquila Sequence	090407174737	2009/04/07 17:47:37,34	42.3295	13.4877	18.5		5.4	5.6
2009	Aquila Sequence	090409005259	2009/04/09 00:52:59,69	42.5013	13.3715	12.7		5.2	5.4
2009	Aquila Sequence	090409193816	2009/04/09 19:38:16,96	42.5178	13.3747	10.5		5.0	5.0
2009	Aquila Sequence	090413211424	2009/04/13 21:14:24,47	42.5122	13.3843	8.3		4.8	4.9

(Continued next page.)

TABLE A1 (continued)
List of the Used Events

Central Italy Data Set

Name of Event		ID	Date and Time (yyyy/mm/dd hh:mm:ss.ss)	Latitude (°)	Longitude (°)	Depth (km)	M_{JMA}	M_w	M_L
2013	Sora (FR)	130216211609	2013/02/16 21:16:09,8	41.7283	13.5870	17.4		4.8	4.8
2013	Costa Marchigiana	130721013224	2013/07/21 10:32:24	43.5398	13.7527	6.0		4.9	5.1
2013	San Gregorio Matese (CE)	131229170843	2013/12/29 17:08:43	41.3767	14.4448	18.7		5.0	5.0
2016	AVN Sequence	160824013632	2016/08/24 10:36:32	42.7002	13.2457	12.2		6.0	6.0
2016	AVN Sequence	160824023328	2016/08/24 20:33:28	42.7990	13.1645	8.9		5.3	5.4
2016	AVN Sequence	160824115030	2016/08/24 11:50:30	42.8265	13.1657	9.3		4.5	4.8
2016	AVN Sequence	160826042825	2016/08/26 04:28:25,91	42.6153	13.2988	6.6		4.8	4.7
2016	AVN Sequence	161026171036	2016/10/26 17:10:36,15	42.8903	13.1373	6.5		0.0	5.6
2016	AVN Sequence	161026191805	2016/10/26 19:18:05,91	42.9120	13.1450	3.5		0.0	5.8
2016	AVN Sequence	161026191807	2016/10/26 19:18:07,42	42.9137	13.1405	3.9		5.9	5.6
2016	AVN Sequence	161026214201	2016/10/26 21:42:01,94	42.8718	13.1248	7.1		4.5	4.7
2016	AVN Sequence	161030064017	2016/10/30 06:40:17,32	42.8397	13.1213	7.6		6.5	6.1
2016	AVN Sequence	161030120700	2016/10/30 12:07:00,21	42.8442	13.0763	8.5		4.5	4.7
2016	AVN Sequence	161103003501	2016/11/03 00:35:01,29	43.0355	13.0622	6.2		4.7	4.9
2017	AVN Sequence	170118092540	2017/01/18 09:25:40,39	42.5597	13.2923	10.2		5.1	5.3
2017	AVN Sequence	170118101409	2017/01/18 01:14:09,9	42.5498	13.2957	10.6		5.5	5.4
2017	AVN Sequence	170118101533	2017/01/18 10:15:33,4	42.5357	13.2970	10.5		0.0	4.5
2017	AVN Sequence	170118101639	2017/01/18 10:16:39,6	42.5487	13.2827	10.4		0.0	4.4
2017	AVN Sequence	170118102523	2017/01/18 10:25:23,73	42.5257	13.2915	10.5		5.4	5.3
2017	AVN Sequence	170118133336	2017/01/18 13:13:36,74	42.4852	13.2765	12.2		5.0	5.2
2018	AVN Sequence	180410031130	2018/04/10 03:11:30,76	43.0718	13.0468	5.4		4.6	4.8
2022	Costa Marchigiana	221109060725	2022/11/09 06:07:25	43.8263	13.1448	4.0		5.5	5.6
2022	Costa Marchigiana	221109060828	2022/11/09 06:08:28	43.8925	13.3167	14.3		0.0	5.3
2023	Umbertide (PG)	230309190805	2023/03/09 19:08:05	43.2842	12.3927	3.3		4.5	4.6
2023	Montagano (CB)	230328215245	2023/03/28 21:52:45	41.6517	14.6477	18.9		4.6	5.0

Manuscript received 29 May 2024
Published online 31 October 2024